0026-895X/02/6103-682–694$3.00
MOLECULAR PHARMACOLOGY
Copyright © 2002 The American Society for Pharmacology and Experimental Therapeutics
Mol Pharmacol 61:682–694, 2002

Vol. 61, No. 3
1090/966220
Printed in U.S.A.

Single-Channel Pharmacology of Mibefradil in Human Native T-Type and Recombinant $Ca_v3.2$ Calcium Channels

GUIDO MICHELS, JAN MATTHES, RENATE HANDROCK, UTE KUCHINKE, FERDI GRONER, LEANNE L. CRIBBS, ALEXEY PEREVERZEV, TONI SCHNEIDER, EDWARD PEREZ-REYES, and STEFAN HERZIG

Departments of Pharmacology (G.M., J.M., R.H., U.K., F.G., S.H.) and Neurophysiology (A.P., T.S.), University of Cologne, Cologne, Germany; Department of Medicine, Cardiovascular Institute, Loyola University, Maywood, Illinois (L.L.C.); and Department of Pharmacology, University of Virginia, Charlottesville, Virginia (E.P-R.)

Received May 8, 2001; accepted December 3, 2001

This article is available online at http://molpharm.aspetjournals.org

ABSTRACT

To study the molecular pharmacology of low-voltage–activated calcium channels in biophysical detail, human medullary thyroid carcinoma (hMTC) cells were investigated using the single-channel technique. These cells had been reported to express T-type whole-cell currents and a $Ca_v3.2$ (or α1H) channel subunit. We observed two types of single-channel activity that were easily distinguished based on single-channel conductance, voltage dependence of activation, time course of inactivation, rapid gating kinetics, and the response to the calcium agonist (*S*)-Bay K 8644. Type II channels had biophysical properties (activation, inactivation, conductance) typical for high-voltage–activated calcium channels. They were markedly stimulated by 1 μM (*S*)-Bay K 8644, allowing to identify them as L-type channels. The channel termed type I is a low-voltage–activated, small-conductance (7.2 pS) channel that inactivates rapidly and is not modulated by (*S*)-Bay K 8644. Type I channels are therefore classified as T-type channels. They were strongly inhibited by 10 μM mibefradil. Mibefradil block was caused by changes in two gating parameters: a pronounced reduction in fraction of active sweeps and a slight shortening of the open-state duration. Single recombinant low-voltage–activated T-type calcium channels were studied in comparison, using human embryonic kidney 293 cells overexpressing the pore-forming $Ca_v3.2$ subunit. Along all criteria examined (mechanisms of block, extent of block), recombinant $Ca_v3.2$ interact with mibefradil in the same way as their native counterparts expressed in hMTC cells. In conclusion, the pharmacologic phenotype of these native human T-type channels—as probed by mibefradil—is similar to recombinant human $Ca_v3.2$.

Nearly 2 decades ago, T-type calcium channels were discovered and described in neurons (Carbone and Lux, 1984) and heart cells (Bean, 1985; Nilius et al., 1985). These low-voltage–activated calcium channels open upon small depolarizations of the membrane potential, inactivate within milliseconds, and have a low single-channel conductance for Ba^{2+}, compared with the high-voltage–activated calcium channels (Bean, 1985; Nilius et al., 1985; Droogmans and Nilius, 1989). T-type calcium channels are found in a variety of tissues in which their role is only partially understood (Vassort and Alvarez, 1994). T-type channels may differ considerably in their pharmacological properties depending on tissue or cell type (Huguenard, 1996).

The molecular composition of the T-type calcium channel was elusive for many years, whereas in the case of high-voltage–activated channels, seven different genes encoding the pore-forming α1 subunit of the channel protein have been defined (α1S and α1A-F). Within the last 3 years, three new α1 subunits were cloned and named the α1G, α1H, and α1I subunits. This corresponds to $Ca_v3.1$, $Ca_v3.2$, and $Ca_v3.3$, respectively, according to the recent nomenclature (Ertel et al., 2000). Extensive whole-cell studies of these recombinant subunits expressed in *Xenopus laevis* oocytes or human embryonic kidney cells reveal typical biophysical characteristics of native T-type calcium channels (Cribbs et al., 1998; Perez-Reyes et al., 1998; Lee et al., 1999), but at the single-channel level, only their conductance has been investigated. Another issue is whether any of the known auxiliary subunits associate with and modulate $Ca_v3.X$ channels. Previous studies did not resolve this question (Dolphin et al., 1999; Lacinova et al., 1999; Klugbauer et al., 2000).

In this study, we explored for the first time single-channel pharmacology of human native T-type and recombinant $Ca_v3.2$ channels. Our rationale was that single-molecule bio-

This study was supported in part by a grant from Roche (Grenzach-Wyhlen, Germany).

ABBREVIATIONS: hMTC, Human medullary thyroid carcinoma (C-) cells; HEK, human embryonic kidney; G418, geneticin; NP_o, open probability of a single channel multiplied by the number of channels in the patch; P_o, open probability of a single channel; f_{active}, fraction of active sweeps; $P_{o,\,active}$, single-channel open probability within active sweeps; i, single-channel current amplitude; I_{peak}, peak value of ensemble average current; TP, test potentials.

physics and their modulation by drugs may give deeper insight into channel behavior and possibly its modulation by as-yet-unknown auxiliary subunits. For the native channels, we used a human cell line [human medullary thyroid carcinoma (hMTC)] because it expresses pure T-type calcium currents at the whole-cell level (Biagi et al., 1992), and because a $Ca_v3.2$ (α1H) channel was cloned from this source (Williams et al., 1999). At least some auxiliary subunits (Hobom et al., 2000) are also expressed in hMTC cells. As a recombinant system, human $Ca_v3.2$ stably overexpressed (Cribbs et al., 1998) in human embryonic kidney (HEK) 293 cells was used in comparison. The main pharmacological tool employed was mibefradil, a known selective nondihydropyridine blocker of native (Mishra and Hermsmeyer, 1994; see also Bezprozvanny and Tsien, 1995) and recombinant (Cribbs et al., 1998) T-type channels. Mibefradil was also of interest because it differentiates between coexpressed auxiliary β-subunits when interacting with another voltage-dependent calcium channel, $Ca_v1.2$ (Welling et al., 1995).

To our initial surprise, a high-voltage–activated calcium channel is also observed in hMTC cells at the single-channel level. We provide evidence that those two channels can easily be discriminated from each other and represent T- and L-type channels, respectively. The single-channel pharmacology of the T-type is extensively analyzed and compared with its recombinant counterpart. We demonstrate that mibefradil blocks both native T-type and recombinant $Ca_v3.2$ channels by two mechanisms (i.e., a reduction of the fraction of active sweeps and a slight reduction of open times).

Materials and Methods

Cell Culture. hMTCcells were grown in RPMI 1640 medium (Biochrom KG, Berlin, Germany) supplemented with 10% fetal bovine serum (Sigma, Deisenhofen, Germany), penicillin (50 units/ml), and streptomycin (50 μg/ml). Cells were plated onto polystyrene dishes. HEK 293 cells have been stable transfected with the human $Ca_v3.2$ without auxiliary subunits as described previously (Cribbs et al., 1998; Lee et al., 1999). Cells were grown in Dulbecco's modified Eagle's medium (Biochrom KG) supplemented with fetal bovine serum (Sigma) and G418 (1 mg/ml; Invitrogen, Karlsruhe, Germany). Cells were grown onto polystyrene dishes coated with 0.1% gelatin, which also served as recording chambers. For electrophysiological experiments, cells were used on the second day (hMTC) or on the first to third day (HEK 293) after plating.

Electrophysiology. Single calcium channels were recorded in the cell-attached configuration of the patch-clamp technique. Experiments were performed in an external solution containing 120 mM K-glutamate, 25 mM KCl, 2 mM $MgCl_2$, 10 mM HEPES, 2 mM EGTA, 1 mM $CaCl_2$, 1 mM Na-ATP, and 10 mM dextrose, pH 7.4. Pipettes (borosilicate glass, 6–7 MΩ) were filled with 110 mM $BaCl_2$ and 10 mM HEPES, pH 7.4. Ba^{2+} currents were elicited by depolarizing test pulses delivered at 0.5 Hz, recorded at 10 kHz and filtered at 2 kHz (−3 dB, four-pole Bessel) using an Axopatch 1D or Axopatch 200 A (Axon Instruments, Union City, CA). The pClamp software (versions 5.5 and 6.0, Axon Instruments) was used for data acquisition and analysis. Drugs were added to the bath as a 20-μl bolus of an appropriate stock solution, assuming a bath volume of 2 ml. At the end of the experiments, the actual bath volume was measured, and the exact drug concentration was calculated. All experiments were carried out at room temperature (21–23°C).

Drugs. Mibefradil was a gift of Hoffmann-La Roche (Basel, Switzerland). It was prepared as a 10 mM stock solution in H_2O, which

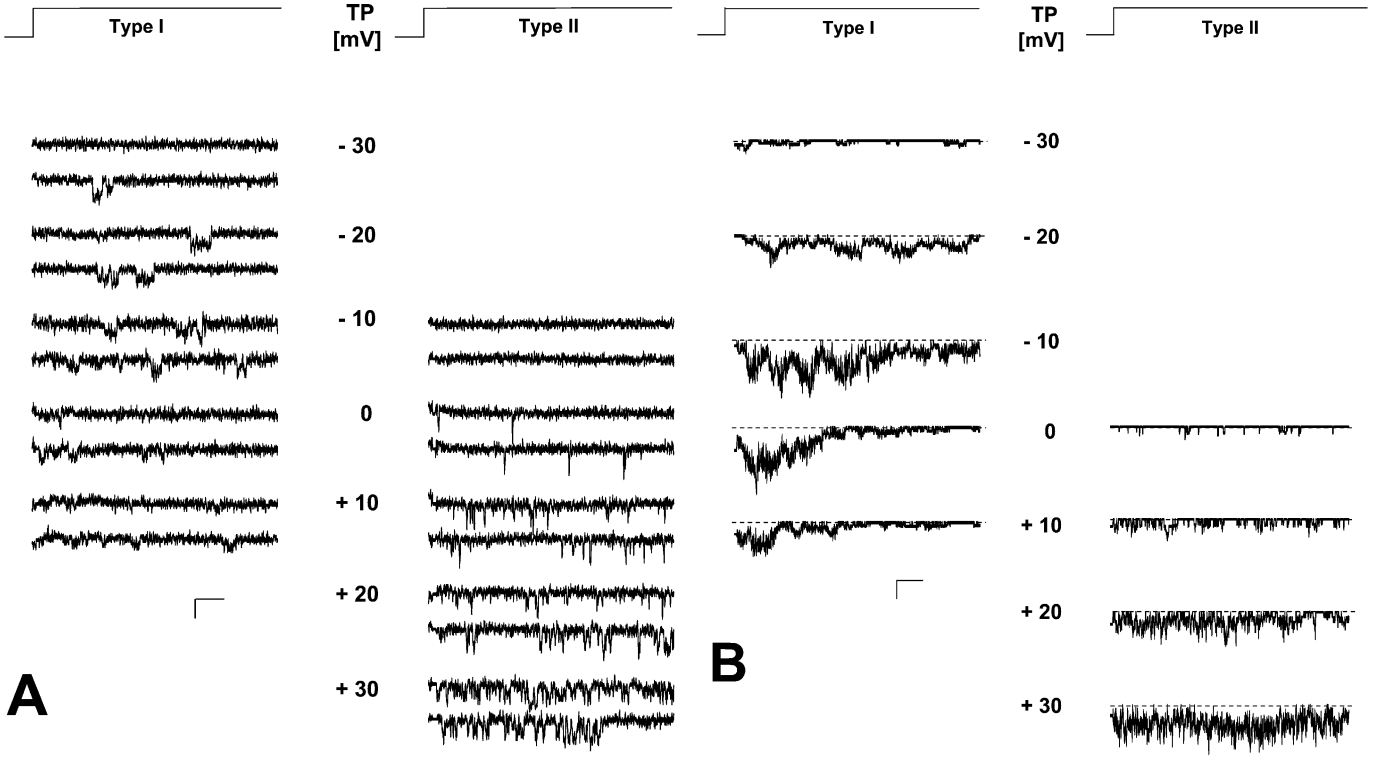

Fig. 1. Original traces (A) and ensemble average currents (B) from two experiments, illustrating the differences between type I and type II channel behavior in hMTC cells. Patches were depolarized from −90 mV to various test potentials (TP), as indicated in the figure. In A, two traces are shown for each indicated TP. Scale bars indicate 15 ms and 0.5 pA, respectively. In B, average currents from 60-sweep ensembles are displayed for various TP. Scale bars indicate 15 ms and 50 fA in this case.

was freshly diluted with bath solution to 0.1 mM on each experimental day. (*S*)-Bay K 8644 (Sigma/RBI, Natick, MA) and nitrendipine (Sigma) were dissolved and stored light-protected in absolute ethanol as 10 mM stock solutions and diluted to 0.1 mM for daily use. The final ethanol concentration in the bath was ≤ 0.11%.

Data Analysis. Linear leak and capacity currents were digitally subtracted using the average currents of nonactive sweeps. Openings and closures were identified using the half-height criterion (pClamp 6.0). For analysis of data obtained with $Ca_v3.2$ we also used custom-made software (*Patch 0.2*) that employs the same idealization algorithm but allows for improved leak subtraction and data-editing features. Data were further analyzed by histogram analysis (see below). Closed time analysis was restricted to patches where only one channel was present. NP_o (the product of the number of channels in the patch times their individual open probability) was calculated as the ratio between the total open time and the total recording time at the test potential. P_o (the single channel open probability) was calculated as the ratio of the total open time and the total time recorded at the test potential, divided by the number of channels in the patch (N) where necessary and possible. f_{active} (the fraction of sweeps containing at least one opening) was corrected by the square-root method: $1 - f_{active,\ corrected} = (1 - f_{active,\ uncorrected})^{1/N}$ for multichannel patches in hMTC cells. The number of channels in the patch was estimated here by dividing the maximum current observed with stacked openings through the unitary amplitude. $P_{o,\ active}$ (the open probability within active sweeps) was computed as the ratio P_o/f_{active}. The voltage-dependence of f_{active} and P_o was analyzed using the Boltzmann function: $Y = Y_{max}/\{1 + e^{(V_{0.5} - V/k)}\}$, where $V_{0.5}$ is the voltage of half-maximal (in)activation and k is the slope factor. Single-channel amplitudes (i) were determined by direct measurements of fully resolved openings or as the maximum of Gaussian fits to all-point amplitude histograms of "semi"-idealized openings [semi-idealized traces: raw data during openings but idealized (zeroed) baseline]. I_{peak} was determined as the maximum of ensemble average currents. The time course of inactivation (τi) was analyzed by fitting nonlinear approximation the ensemble average current I to the equation $I_{(t)} = I_{max.} \times (1 - e^{-t/\tau a})^2 \times e^{-t/\tau i}$ (Droogmans and Nilius, 1989; Huguenard, 1996). A two-tailed t test was used for statistical examinations, using unpaired format for comparison of different channels and paired format for testing drug effects. A value of $p < 0.05$ was considered significant. Data are given as means ± S.E.M. Open-time constants (τ_{open}) were obtained from single experiments using simple exponential fits of open-time histograms by maximum likelihood method. Single τ values were averaged as pooled mean according to the equation $\tau_{open,\ pooled} = [\Sigma((\tau_e)\cdot(1/SD_e^2))/(\Sigma(1/SD_e^2))]$, where SD_e is the individual standard deviation. SD_e was estimated by $SD_e = \tau_e/n^{1/2}$, where τ_e is the estimated open-time constant and n means the number of events used for estimation of τ_e. Standard deviation of the pooled mean ($\tau_{open,\ pooled}$) was then calculated from $SD_{pooled}^2 = 1/(\Sigma(1/SD_e^2))$. Average means of open-time constants were compared using the unpaired two-tailed t test.

Results

In cell-attached recordings, we obtained two visually distinct types of single-channel activity, which we initially

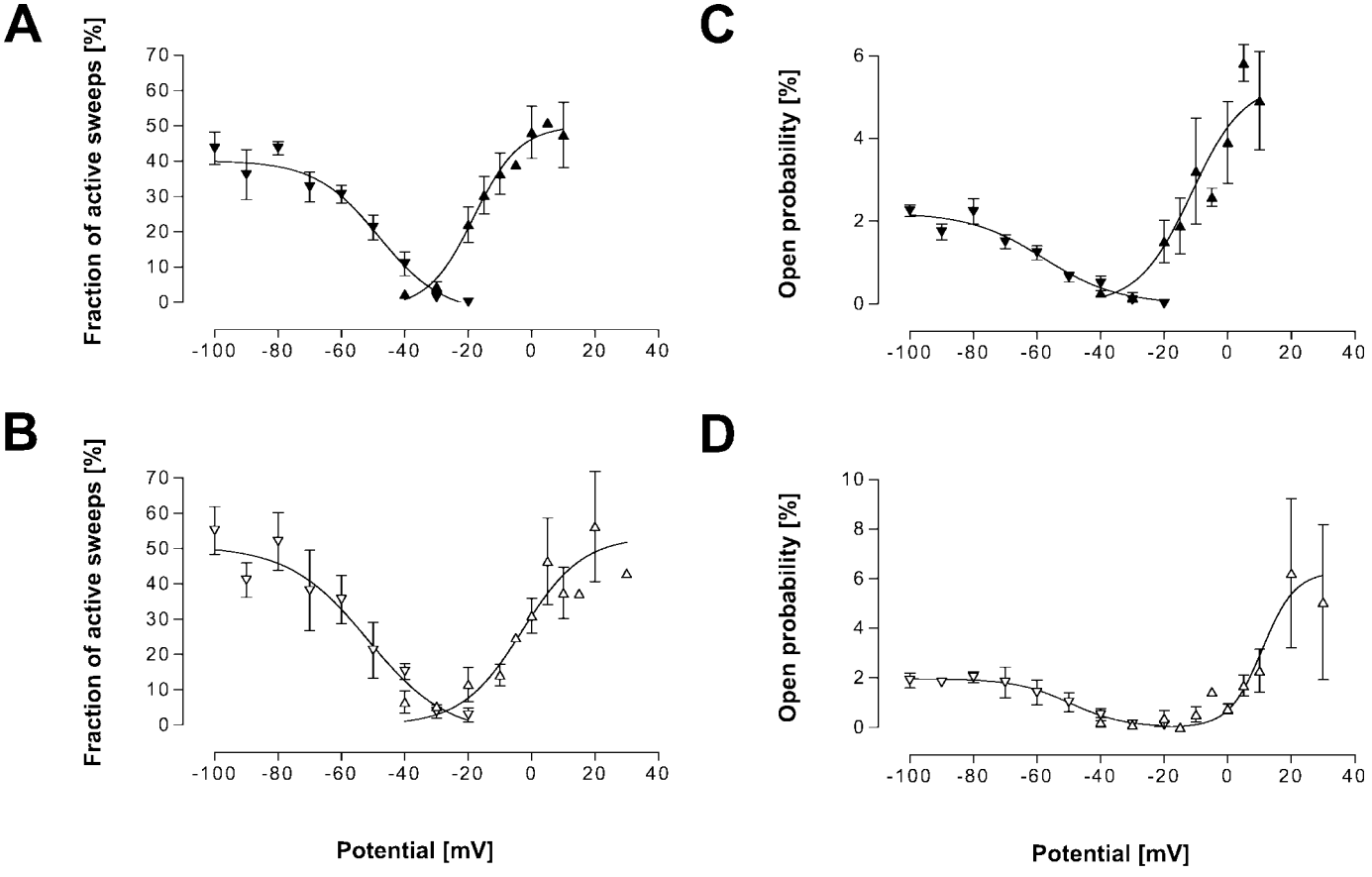

Fig. 2. Voltage-dependence of single-channel activity of type I (A and C) and type II (B and D) channels in hMTC cells. Patches were depolarized every 2 s from −90 mV to various test potentials (activation), or from various holding potentials (inactivation) to −10 mV (A and C) or +10 mV (B and D). Data were averaged from $n = 10$ (A, activation), 8 (A, inactivation), 10 (B, activation), 7 (B, inactivation), 10 (C, activation), 9 (C, inactivation), 9 (D, activation), and 7 (D, inactivation) experiments. The curves shown here were fitted using the Boltzmann equation and the pooled data as displayed. Mean values as indicated in the text were derived from Boltzmann fits of individual experiments.

termed "type I" and "type II" behavior. Representative examples from two experiments are compiled in Fig. 1. At first glance, types I and II differ in at least four different aspects. For type I, it activates at lower voltages, it has a lower single-channel amplitude at any given test potential, openings occur in well-separated bursts at any given test potential, and the ensemble average current inactivates rapidly. For type II, openings are more evenly distributed, and average currents do not visibly undergo time-dependent inactivation. We will systematically compare these properties one by the other in the following.

The voltage-dependences of activation and inactivation were analyzed by plotting f_{active} (measured from at least 60 test pulses) against the voltage of the test potential or holding potential, respectively. The pooled data are shown in Fig. 2, A and B. Individual type I channels activate half-maximally at -17.7 ± 2.9 mV, with a slope factor of 4.3 ± 1.0 mV ($n = 4$). Half-maximal inactivation occurs at -51.1 ± 3.5 mV with a slope of -7.6 ± 1.4 mV ($n = 7$). A small window current is suggested by the overlap of these curves between -40 mV and -20 mV (Cribbs et al., 1998). For type II, inactivation lies in the same order of magnitude ($V_{0.5}$, -48.8 ± 2.3 mV; slope, -7.9 ± 0.7 mV; $n = 3$), but activation occurs at much more positive potentials ($V_{0.5}$, -8.0 ± 0.9 mV; slope, 7.5 ± 2.0 mV; $n = 4$, $p < 0.05$). Maximum f_{active} was always $\approx 50\%$. When analyzing P_o in a similar manner (Fig. 2, C and D), the maximum values of activation curves were more variable, and saturation was not clearly evident at the most positive test potentials where openings still could be resolved (Cachelin et al., 1983). Yet, potentials of half-maximum activation and inactivation gave results consistent with f_{active} for both type I (activation: $V_{0.5}$, -13.9 ± 4.7 mV; slope, 4.9 ± 0.6 mV; $n = 6$; inactivation: $V_{0.5}$, -66.3 ± 4.6 mV; slope, -12.5 ± 3.1 mV; $n = 5$) and type II (activation: $V_{0.5}$, 17.9 ± 5.2 mV; slope, 7.2 ± 0.7 mV; $n = 5$; inactivation: $V_{0.5}$, -45.8 ± 4.9 mV; slope, -6.9 ± 2.5 mV; $n = 4$) channels, respectively.

The difference between type I and type II regarding single-channel conductance is illustrated in Fig. 3. Type I channels (closed symbols) have a lower single-channel current amplitude at any given test potential, and the slope conductance, calculated individually by linear regression, is significantly lower, too (type I, 7.2 ± 0.6 pS, $n = 10$; type II, 14 ± 1 pS, $n = 10$).

The most prominent difference regarding rapid gating was the bursting pattern of openings, which was evident over the whole voltage range in the case of type I channels. Therefore, we analyzed the closed-time distribution of type I and II channels at a test potential of 0 mV, where single-channel events could still be resolved for type I channels, and channel activity was already substantial for type II (see Fig. 1). As seen in Fig. 4, both channel types clearly reveal two components in their closed-time histograms. The slow component had a comparable time constant, τ_2, that amounted to 22.1 ± 4.2 ms ($n = 4$) for type I and 22.0 ± 2.8 ms ($n = 5$) for type II channels. The τ_1 extrapolated from maximum likelihood fits,

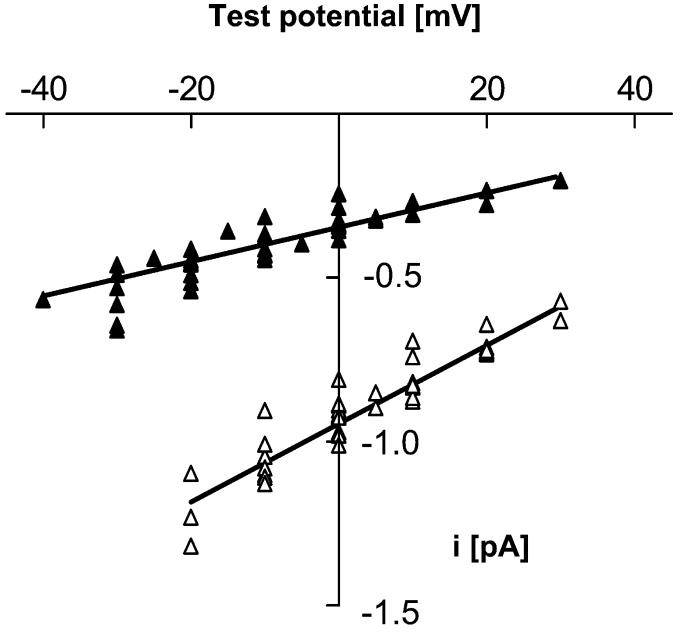

Fig. 3. Single-channel amplitude i of type I (closed symbols, $n = 10$) and type II (open symbols, $n = 10$) channels as a function of test potential. Holding potential was -90 mV throughout. Values of i were measured using fully resolved openings. Slope conductances as depicted here were calculated based on pooled data from type I and type II channels, respectively. See text for average values determined by linear regression in each individual experiment.

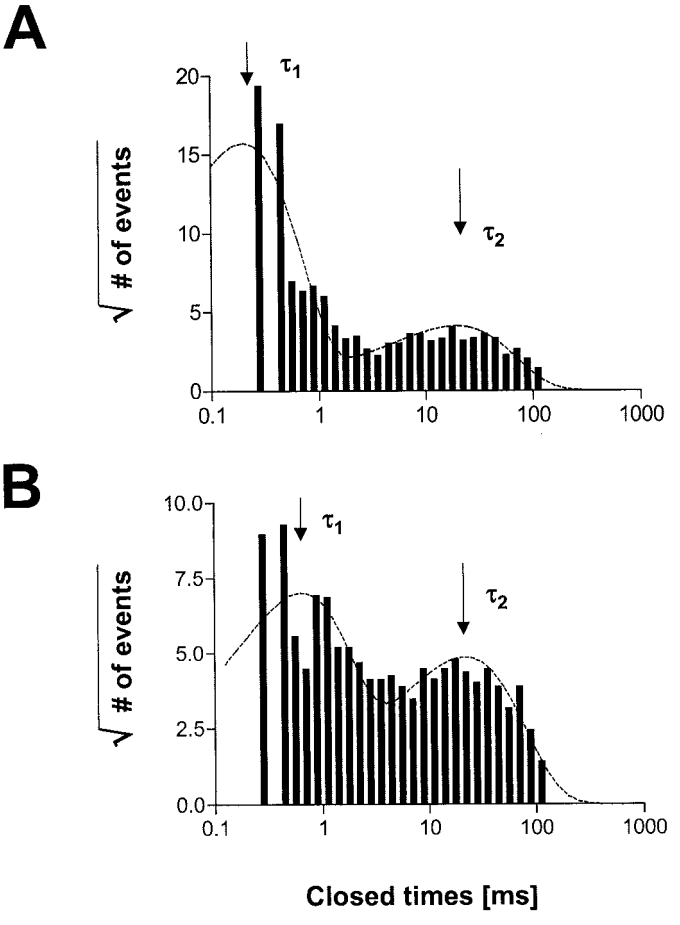

Fig. 4. Closed-time distribution of type I (A) and type II (B) channels, obtained at a test potential of 0 mV (holding potential -90 mV). Data (plotted according to Sigworth and Sine, 1987) were pooled from one-channel experiments ($n = 4$ and 5, respectively), where the amount of data allowed for individual maximum likelihood estimation of the τ_1 and τ_2 values (see text). Dotted lines represent maximum likelihood fits of the pooled data as displayed.

however, seemed shorter in type I (0.20 ± 0.01 ms) than in type II (0.60 ± 0.11 ms). Furthermore, the computed size of the fast component seemed to be more prominent in the case of type I channels. Taken together, these two features illustrate the clear-cut bursting pattern of type I activity. They translate into a markedly, significantly shorter overall mean closed time (type I, 0.79 ± 0.20 ms, $n = 6$; type II, 9.22 ± 1.72 ms, $n = 7$).

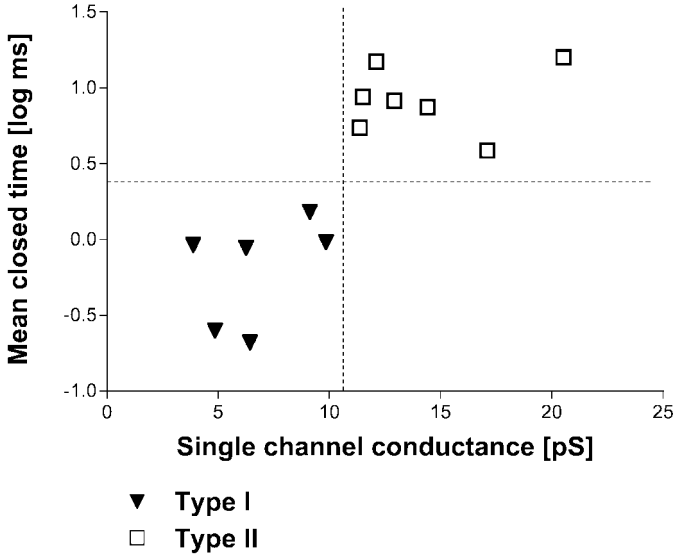

Fig. 5. Comparison between channels classified visually as type I (▼, $n = 6$) and type II (□, $n = 7$) using two independent biophysical criteria: conductance (abscissa, see Fig. 3) and mean closed time (ordinate, see Table 1). Only one-channel patches were included. There is no overlap between the values covered by each criterion, and there is no case of ambiguity, as indicated by the two empty quadrants.

A rapid inactivation during the test pulse was regularly observed for type I channels but not type II channels. For a number of experiments like those shown in Fig. 1, we were able to analyze the voltage-dependence of the inactivation time course (τi) by nonlinear approximation (see *Materials and Methods*). In the case of type I, inactivation was fast and accelerated by more positive test voltages: the τi values were 62 ± 23 ms, 31 ± 11 ms, and 31 ± 2 ms ($n = 3$–5) at voltages of −10 mV, 0 mV, and +10 mV, respectively. In contrast, τi values increased with voltage in the case of type II: 62 ± 3 ms at 0 mV, 77 ± 13 ms at +10 mV, 349 ± 126 ms at +20 mV, and 458 ± 120 ms at +30 mV ($n = 3$–4). Further examples illustrating the different inactivation behavior can be seen in Figs. 6 and 7.

To exclude the possibility that our analysis of type I versus type II channels is biased by a selection artifact, we checked our identification by plotting two of the proposed distinctive biophysical features against each other (Fig. 5), single-channel conductance and mean closed time (at 0 mV, from one-channel patches only). It can be seen that there is no single case of overlap between those two parameters, which are not inherently dependent on each other.

In a second series of experiments, we tested our hypothesis that type I and II channels represent different entities by

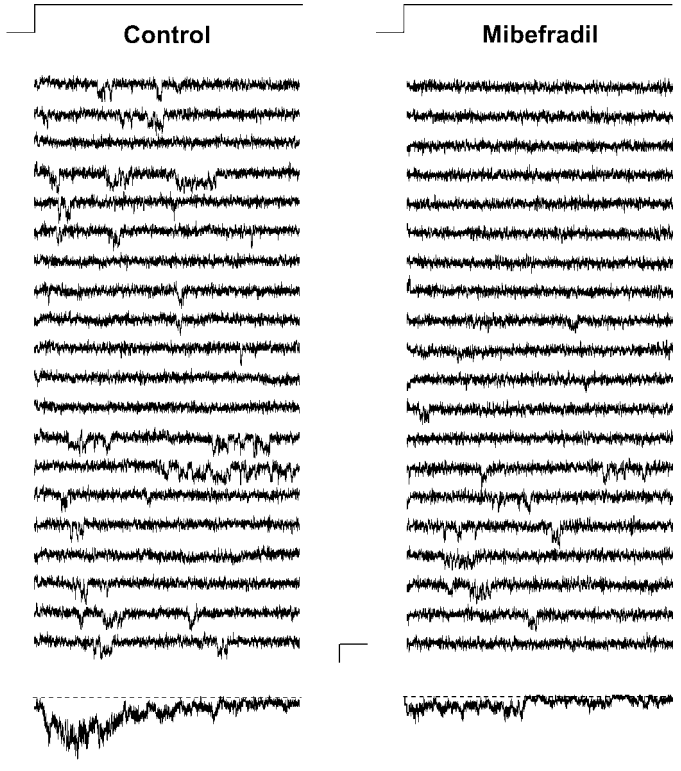

Fig. 6. Inhibition of a type I channel (control, left) by mibefradil (right). The top illustrates the pulse protocol (holding potential −90 mV, test potential −10 mV). The bottom trace depicts ensemble averages from 235 traces before drug and 174 traces after drug. The middle shows consecutive sweeps. Scale bars indicate 15 ms and 1 pA (individual traces) or 20 fA (ensemble averages), respectively.

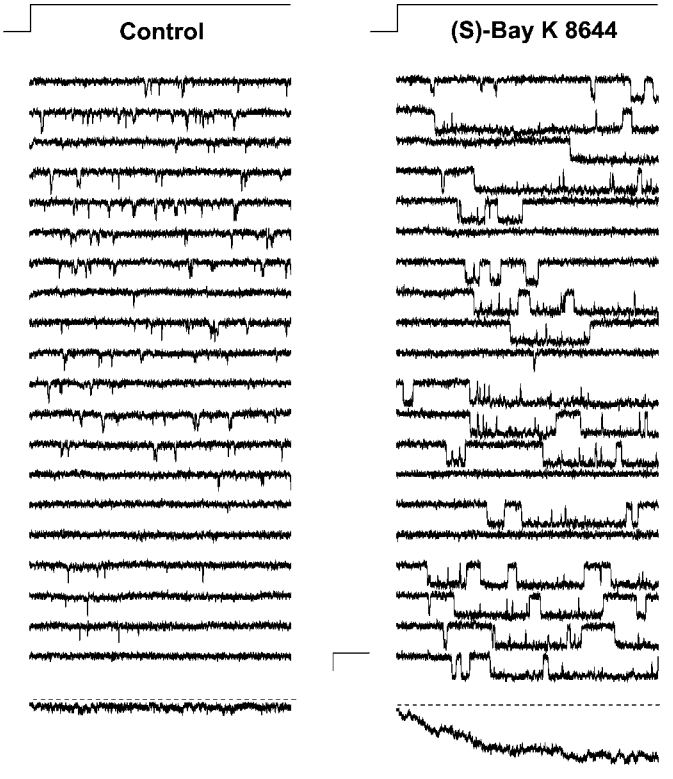

Fig. 7. Stimulation of a type II channel (control, left) by (*S*)-Bay K 8644 (right). The top illustrates the pulse protocol (holding potential −90 mV, test potential +10 mV). The bottom trace depicts ensemble averages from 117 traces before drug and 179 traces after drug. The middle shows consecutive sweeps. Scale bars indicate 15 ms and 1 pA (individual traces) or 75 fA (ensemble averages), respectively. Besides a prominent increase in open times and open probability (see Table 1), the drug enlarged single-channel amplitude (from 0.89 ± 0.04 pA to 1.13 ± 0.09 pA). Conductance was raised to 23.1 ± 1.0 pS ($n = 9$).

using a pharmacological approach. Channels were classified as type I or II during the early course of the experiments according to the criteria mentioned above. Type I channels were then step-depolarized to −10 mV (Fig. 6) and type II channels to +10 mV (Fig. 7), offering optimal activity and recording conditions for each case. After a control period, channels were then exposed to either solvent, the L-type calcium-channel agonist (*S*)-Bay K 8644, or the T-type channel blocker mibefradil. Under control conditions, type II but not type I channels underwent some decline in activity ("run

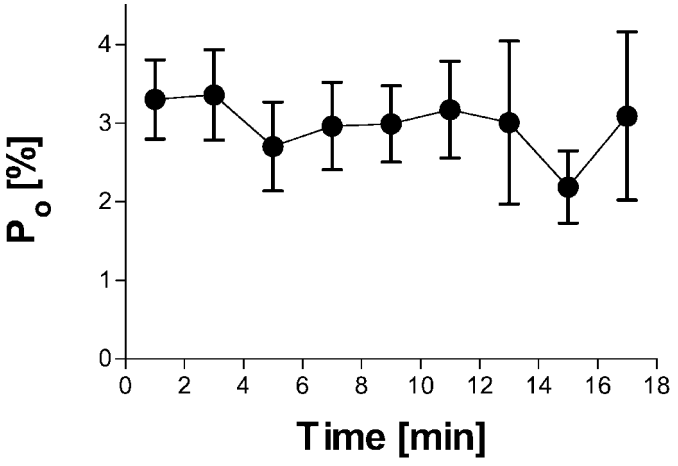

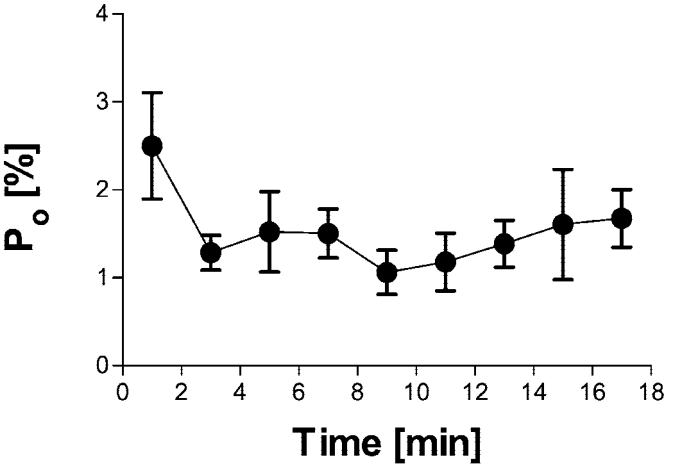

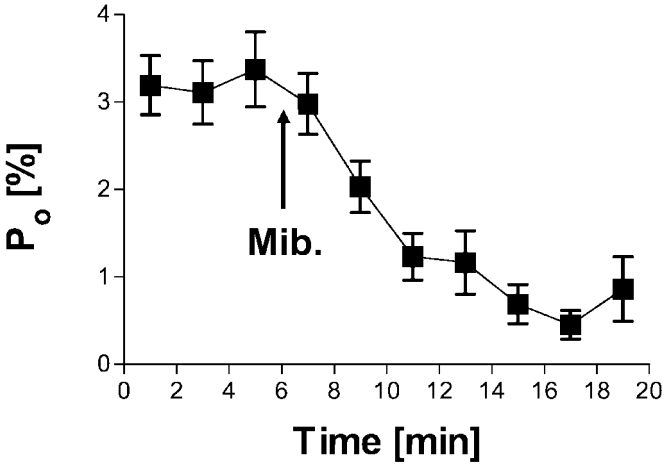

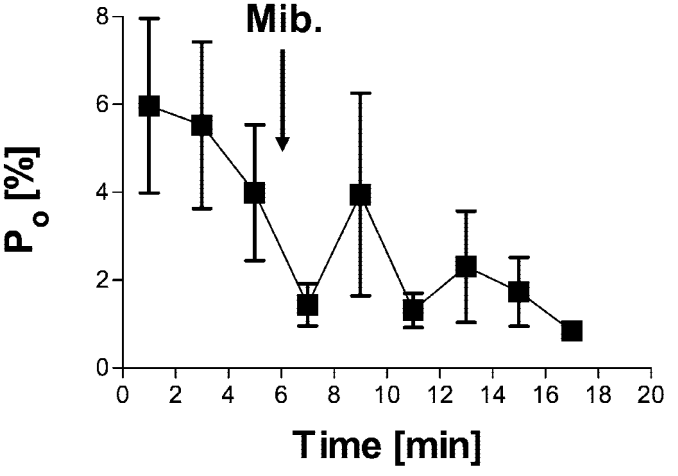

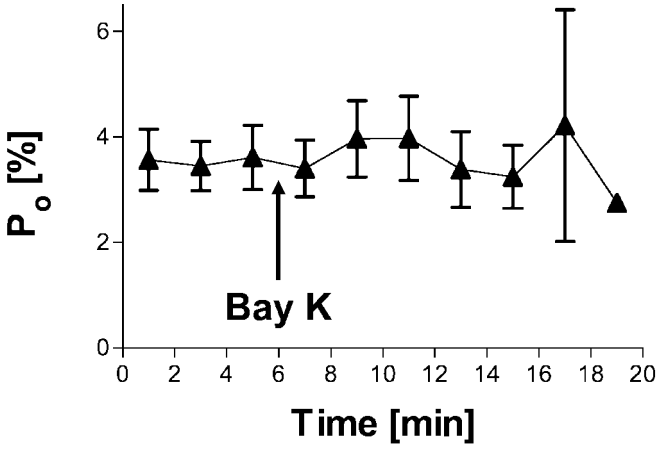

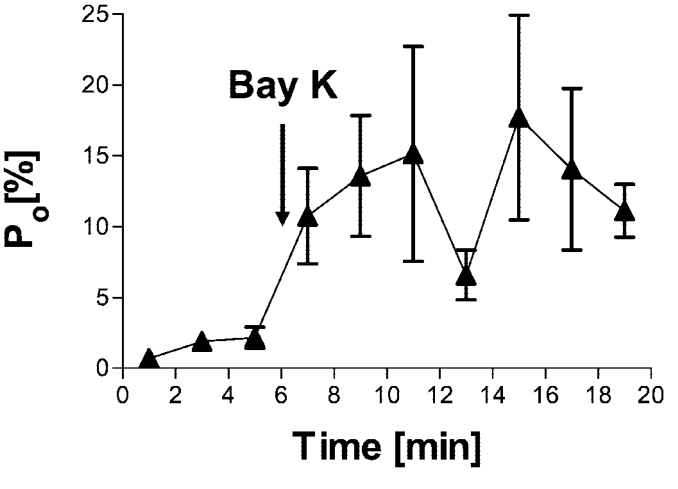

Fig. 8. Open probability P_o (averaged over 2-min recording periods) of type I channels versus time. Channels were depolarized to −10 mV and exposed after 6 min to solvent (top, $n = 8$), mibefradil (middle, 10.0 ± 0.1 μM, $n = 13$), or (*S*)-Bay K 8644 (bottom, 1.02 ± 0.01 μM, $n = 10$).

Fig. 9. Open probability P_o (averaged over 2-min recording periods) of type II channels versus time. Channels were depolarized to +10 mV and exposed after 6 min to solvent (top, $n = 10$), mibefradil (middle, 9.7 ± 0.3 μM, $n = 7$), or (*S*)-Bay K 8644 (bottom, 1.01 ± 0.01 μM, $n = 9$).

down", see Figs. 8 and 9). The time course of P_o observed after drug application is depicted in Figs. 8 and 9. The most prominent drug effects were profound inhibition of type I by mibefradil (10.0 ± 0.1 μM; Fig. 8, middle), and stimulation of type II by (*S*)-Bay K 8644 (1.01 ± 0.01 μM; Fig. 9, bottom) because of an increase in open times and therefore in open probability within active sweeps ($P_{o,\ active}$, Table 1). (*S*)-Bay K 8644 (1.02 ± 0.01 μM) had no effect on type I channels. Mibefradil (9.7 ± 0.3 μM) inhibited I_{peak} of type II channels by 50% of predrug values. This effect was caused by a corresponding change in f_{active}, whereas open times remained unaffected.

In contrast, mibefradil effects on type I channel ensemble average current are composed of two components. First, the fraction of active sweeps again is strongly depressed; in addition, open probability within active sweeps is also reduced to a significant extent, because of a corresponding change in mean open times (Table 1). To address these two components of inhibition in a more quantitative manner, further analysis was performed. The slow gating kinetics of channel "availability" (i.e., transitions between active and nonactive, or blank sweeps), can be analyzed by sweep histogram analysis (Herzig et al., 1993). Blank-sweep histograms were constructed by plotting the cumulative probability density function of series of continuously nonactive sweeps. In the seven experiments with one type I channel in the patch, blank-sweep histograms were well characterized by a single exponential component before mibefradil was applied. The time constant of the underlying nonactive state amounted to τ = 2.68 ± 0.26 s. When data from the seven experiments were pooled (1611 sweeps in total), a similar τ value of 2.66 s was obtained (Fig. 10 A). After application of 10 μM mibefradil, a second, slow component became obvious, τ_2 = 22.1 ± 4.8 s (n = 7) together with the faster component, the τ_1 (2.84 ± 0.36 s, n = 7), which matched the τ value obtained under control conditions (see above). Again, results from the pooled analysis (Fig. 10B) were similar (τ_1 = 2.82 s; τ_2 = 16.7 s). This indicates that fraction of active sweeps is reduced by mibefradil because the channel occasionally adopts a long-lived nonactive, blank state. The lifetime of this state can be taken as a measure of the rate of dissociation of the drug ($1/\tau \approx$ 0.05/s).

Open-time histograms confirm the significant effect of mibefradil seen on mean open time (Table 1). As exemplified in Fig. 11, the dwell time of the open state is adequately described by a single exponential. τ_{open} was reduced from 0.48 ms to 0.37 ms in the case depicted and from 0.50 ± 0.01 ms to 0.43 ± 0.03 ms ($p < 0.05$, n = 13; $\tau_{open,\ pooled}$ ± $S.D._{pooled}$) on average. A clear decrease of τ_{open} was observed in nine experiments (by 24.8 ± 3.5%). The results obtained from open-times analysis indicate that mibefradil exerts an additional effect on the short (millisecond) time scale of single-channel gating. The fact that open probability within active sweeps ($P_{o,\ active}$) and open times are reduced to a similar extent (about −20%, Table 1), together with a lack of effect on closed times, is also compatible with the idea that the drug leads to a rapid, short-lived block of channels on the order of < 1 ms.

HEK 293 cells expressing $Ca_v3.2$ channels were first examined using a pulse protocol in which channels were fully available (holding at −90 mV, test pulses to −20 mV). This gave rise to large, rapidly activating and inactivating currents (Fig. 12 A), but clear-cut unitary events were discernible only during the second half of the test pulse. Every single trace—with some variance regarding peak amplitude—resembled the current wave form obtained by averaging the whole ensemble (Fig. 12A, bottom trace). Mibefradil (10 μM; 8.9 ± 0.6 μM, n = 5) considerably reduced channel activity regarding peak currents. Open probability was markedly reduced, such that nonstacked unitary events were now also observed early in the pulse (Fig. 12 B). The ensemble averages still revealed the typical features of a rapidly activating and inactivating channel. Mibefradil lowered the maximum ensemble average current (I_{peak}) significantly from −567 ± 122 to −189 ± 40 fA. Hence, overexpression had led to a high channel density in every patch examined, and we made no further attempts to characterize single-channel gating (or mibefradil effects) under the conditions of this voltage protocol.

Instead, depolarizing steps from −50 to −20 mV were

TABLE 1

Single-channel mechanism of drug modulation in hMTC cells

Effects of solvent, mibefradil (type I, 10.0 ± 0.1 μM; type II, 9.7 ± 0.3 μM), and (S)-Bay K 8644 (type I, 1.02 ± 0.01 μM; type II, 1.01 ± 0.01 μM) on single-channel parameters of type I and II channels in hMTC cells. Data were collected from 0 to 6 min of recording for the first period and from 7 min to the end of experiments for the second period in the case of (*S*)-Bay K 8644 and solvent. For mibefradil experiments, the first 4 min after application were excluded to allow analysis of the steady-state drug effect (see Figs. 8 and 9). I_{peak} was measured from ensemble average currents, f_{active} represents the fraction of active sweeps, open and closed times were averaged from all detected events, and $P_{o,\ active}$ was calculated as the open probability within active sweeps.

	I_{peak}	f_{active}	Mean open time	Mean closed time	$P_{o,\ active}$	n
	fA	%	*ms*		%	
Type I						
control	−25 ± 3	37 ± 3	0.51 ± 0.04	1.1 ± 0.5	5.2 ± 0.4	8
solvent	−24 ± 5	36 ± 4	0.52 ± 0.05	0.9 ± 0.2	5.1 ± 0.4	8
control	−33 ± 4	43 ± 3	0.63 ± 0.03	1.1 ± 0.2	5.2 ± 0.4	13
Mibefradil (10 μM)	−16 ± 3*	17 ± 3*	0.53 ± 0.05*	1.0 ± 0.2	4.0 ± 0.4*	13
control	−24 ± 2	39 ± 2	0.52 ± 0.03	0.9 ± 0.4	5.5 ± 0.3	10
(*S*)-Bay K 8644 (1 μM)	−26 ± 3	39 ± 3	0.55 ± 0.05	0.8 ± 0.2	5.2 ± 0.3	10
Type II						
control	−18 ± 3	59 ± 6	0.38 ± 0.04	8.1 ± 2.0	2.6 ± 0.4	10
solvent	−15 ± 3	57 ± 8	0.43 ± 0.04	9.5 ± 1.2	2.3 ± 0.2	10
control	−28 ± 5	74 ± 2	0.35 ± 0.01	7.7 ± 1.6	3.9 ± 0.9	7
Mibefradil (10 μM)	−14 ± 2*	44 ± 4*	0.35 ± 0.05	7.2 ± 2.6	2.4 ± 0.4	7
control	−15 ± 3	46 ± 8	0.44 ± 0.06	13.3 ± 1.5	2.3 ± 0.5	9
(*S*)-Bay K 8644 (1 μM)	−105 ± 25*	46 ± 6	3.03 ± 0.54*	7.1 ± 2.5	14.6 ± 2.9*	9

*, a significant difference ($p < 0.05$) between the first and second period.

chosen to induce voltage-dependent steady-state inactivation, which dramatically minimized the number of simultaneously available channels, compared with a holding potential of −90 mV. This made it possible to detect and analyze separate unitary events in both the absence and the presence of mibefradil (Fig. 13). Stacked openings of twice the unitary amplitude were rarely observed. Channel activity remained stable over time in cells not exposed to drug (Fig. 14, top). In the presence of 10 μM mibefradil (9.3 ± 0.5 μM, $n = 8$), the peak inward current obtained from ensemble averages was found to decrease significantly from −46 ± 5 fA to −24 ± 4 fA. In view of the (sub)micromolar IC_{50} values reported for mibefradil in whole-cell studies on $Ca_v3.2$ (Cribbs et al., 1998; Williams et al., 1999) we tested a lower concentration of 3.3 ± 0.1 μM (Table 2). This concentration caused qualitatively similar but smaller effects (I_{peak}, from −93 ± 24 fA to −69 ± 24 fA; NP_o, from 11 ± 3.2% to 7.0 ± 2.9%, $p < 0.05$, $n = 6$). Selectivity of the action of 10 μM mibefradil on these channels was further examined by applying the same concentration of nitrendipine (10.3 ± 0.2 μM, $n = 6$), a selective blocker of single L-type calcium channels (Kawashima and Ochi, 1988). As expected, $Ca_v3.2$ channels were not blocked significantly by this compound (Fig. 14; Table 2).

The mechanism of inhibition by 10 μM mibefradil was now studied in more detail at the single-channel level. As illustrated in Fig. 13, the number of sweeps containing channel activity f_{active} was significantly lowered by 10 μM mibefradil from 67 ± 5 to 40 ± 5%. It should be noted that these numbers only give a lower-limit estimate for the effect on true f_{active} of each single channel involved, because we are unable to determine the total number of channels participating in channel activity. For similar reasons, open probability is indicated here as the conventional raw NP_o [i.e., the product of the (unknown) number of channels times their individual open probability (not corrected for true f_{active}, unlike the data obtained from hMTC cells)]. This parameter—which combines drug effects on f_{active} and those on rapid gating during the available state—was decreased by 10 μM mibefradil from 2.5 ± 0.2 to 1.1 ± 0.2% ($p < 0.05$), hinting at an additional effect on rapid gating. Indeed, mean open times tended to decrease after mibefradil (from 0.73 ± 0.09 ms to 0.63 ± 0.08 ms, see Table 2). Analysis of open-time histograms (Fig. 15) confirmed this tendency: 10 μM mibefradil decreased open-time constants (τ_{open}) from 0.59 ms to 0.45 ms in the case depicted and from 0.45 ± 0.03 ms to 0.39 ± 0.02 ms ($p < 0.05$, $n = 8$, $\tau_{open,\ pooled}$ ± $S.D._{pooled}$) on average. Note that in five experiments, τ_{open} dropped clearly (by 24.2 ± 7.5%). We were concerned that the drug effect on open

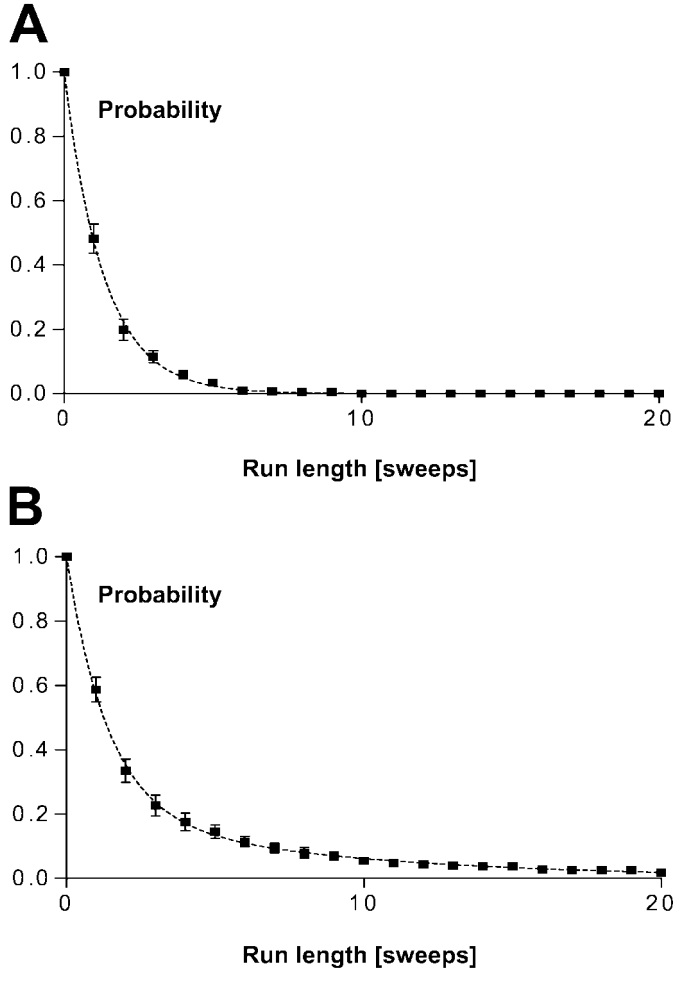

Fig. 10. Blank-sweep histogram from seven one-channel experiments before (A) and after (B) exposure to mibefradil. The drug induces long series of continuously blank sweeps, which constitute a second, long-lived component of the histogram in B (see text).

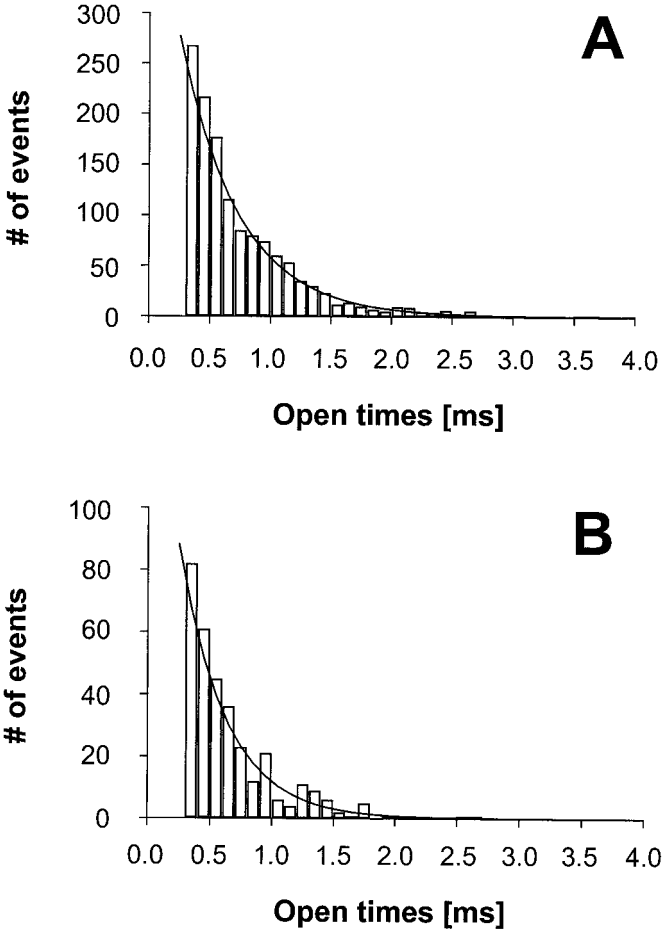

Fig. 11. Open-time histogram from a type I channel before (A) and after (B) exposure to mibefradil. Test potential was −10 mV. The maximum likelihood fit reveals a single exponential open-state component, the lifetime τ_{open} of which is shortened (from 0.48 ms to 0.37 ms in this experiment) by the drug.

times could be artificial, because of fusion of sequential openings of distinct channels (by bandwidth-induced absences of very short closures or very short stacked events). This problem, however, should be less severe during the second half of the test pulses, where openings are very rare and fusion rather unlikely. Indeed, when studying the second half of test pulses, the mibefradil effect on mean open times was well preserved (from 0.76 ± 0.10 ms to 0.64 ± 0.09 ms, $p = 0.06$, $n = 8$).

To examine the possibility of an additional, very rapid block in the range of microseconds, we constructed all-point histograms (Fig. 16) from raw data after semi-idealization of the data sets (see *Materials and Methods*). Single-channel amplitude, as determined by Gaussian fits to the nontruncated portion of histograms, remained unaffected by 10 μM mibefradil both in native (Fig. 16A, control: −0.40 ± 0.02 pA; B, after mibefradil: −0.41 ± 0.03 pA, $n = 13$, n.s.) and in recombinant channels (Fig. 16C, control: −0.41 ± 0.01 pA; D, after mibefradil: −0.42 ± 0.02 pA, $n = 8$, n.s.).

In summary, mibefradil exerted a dual mechanism of block, affecting f_{active} and open times, in $Ca_v3.2$ channels. The "pharmacological phenotype" of the recombinant channels—as far as it can be resolved by analysis of multichannel patches—is therefore indistinguishable from its native counterpart expressed in hMTC cells.

Discussion

The main results of this study are that two types of single calcium channels are present in a human C-cell tumor line (hMTC), that these channels can easily be distinguished by their biophysical properties, that these channels fulfill the necessary criteria to be classified as T-type or L-type channels respectively, that mibefradil blocks T-type channels by reducing fraction of active sweeps and open times, but not single-channel amplitude, and that mibefradil effects are identical when studied in recombinant $Ca_v3.2$ channels.

The large-conductance channel (type II) inactivates slowly (Fig. 1B) and activates at high voltages (Fig. 2B). The voltage-dependence of activation and inactivation, measured under continuous pulsing rather than with conventional two-pulse protocols, is reminiscent of native cardiac human L-type channels (Handrock et al., 1998; Kreuzberg et al., 2000). The single-channel conductance under basal conditions (≈14 pS) does not discriminate between various members of the high-voltage–activated channel family, but conductance can be more accurately determined using the well-resolved openings in the presence of the calcium-channel agonist (*S*)-Bay K 8644 (Fig. 7). The value obtained here (23 pS) is in line with reports on L-type channels (McDonald et al., 1994) under similar conditions, and such an increase found with calcium agonists has been noted previously (Lacerda and Brown, 1989; Handrock et al., 1998; Kreuzberg et

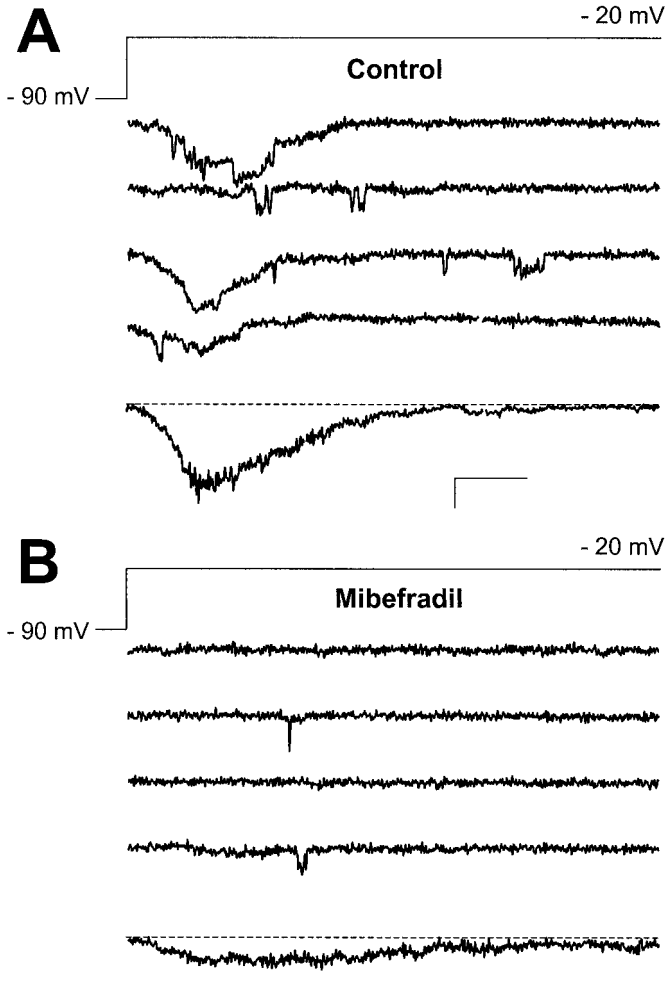

Fig. 12. Single-channel records from an experiment with $Ca_v3.2$ expressing HEK 293 cells. The top illustrates the pulse protocol (holding potential −90 mV, test potential −20 mV). Four sequential traces are shown in the center, whereas the bottom displays the ensemble average current. Scale bars indicate 20 ms and 1 pA for single traces and 200 fA for ensemble averages, respectively. A, control before mibefradil. B, traces obtained in the presence of mibefradil (10 μM).

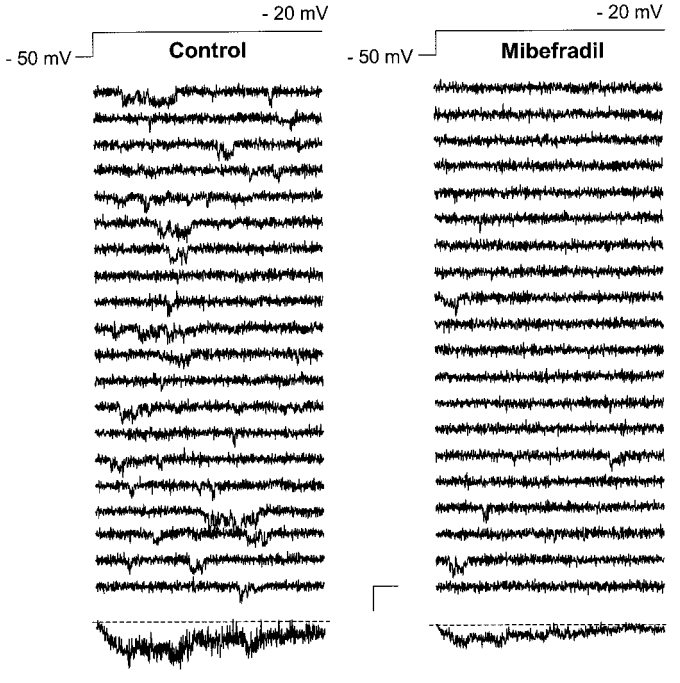

Fig. 13. Blockade of $Ca_v3.2$ channels in HEK 293 cells. As in Fig. 12, the top indicates the pulse protocols (−50 mV holding potential, −20 mV test potential). The bottom trace indicates ensemble average currents before ($n = 240$ sweeps) and after ($n = 418$ sweeps) mibefradil application (10 μM). Left, control before mibefradil; right, traces obtained in the presence of mibefradil (10 μM). Scale bars indicate 15 ms and 1 pA (individual traces) or 20 fA (ensemble average currents).

al., 2000). Importantly, a stimulatory response to calcium agonists per se (Figs. 7 and 9) is a hallmark feature of L-type (Hess et al., 1984) but not other types of voltage-activated calcium channels. In characteristic distinction (Nilius et al., 1985; McDonald et al., 1994) to the low-voltage–activated channel we observed, type II channels exhibited time-dependent loss of activity [i.e., "run down" (Figures 8 and 9)]. On the basis of our results, the molecular entity (α1C, α1D, α1F, or α1S, corresponding to $Ca_v1.2$, $Ca_v1.3$, $Ca_v1.4$, and $Ca_v1.1$, respectively) that represents the pore-forming unit cannot be determined, although the source of cells (endocrine) favors the first two possibilities (Ertel et al., 2000). Furthermore, it remains unclear why previous investigators did not detect an L-type current at the whole-cell level (Biagi et al., 1992; but see Mehrke et al., 1994), despite the observation that hormone secretion in primary human MTC-cells is stimulated and inhibited by dihydropyridine agonist and antagonist, respectively (Raue et al., 1989). We observed marked periodic changes in the occurrence of type II, but not type I, channels over the course of the project, which were independent of passage number or batch of cells (not shown). The inhibition of the L-type channel by mibefradil, known from other systems (e.g., Bezprozvanny and Tsien, 1995; Welling et al., 1995) but seen here for the first time with single channels, merits further analysis once the molecular channel entity is identified (see above).

The type I behavior reported here fulfills all tested criteria of a T-type, $Ca_v3.X$ channel, namely activation in the low-voltage range (Figs. 1–3) and low conductance of 7 to 8 pS (Fig. 3) with isotonic Ba^{2+} (Nilius et al., 1985; note that the lower value of 5.3 pA reported by Cribbs et al., 1998, was obtained at much more negative potentials), fast inactivation (Fig. 1B), and sensitivity toward mibefradil (Cribbs et al., 1998). Deactivation was not studied here, as the long pulses

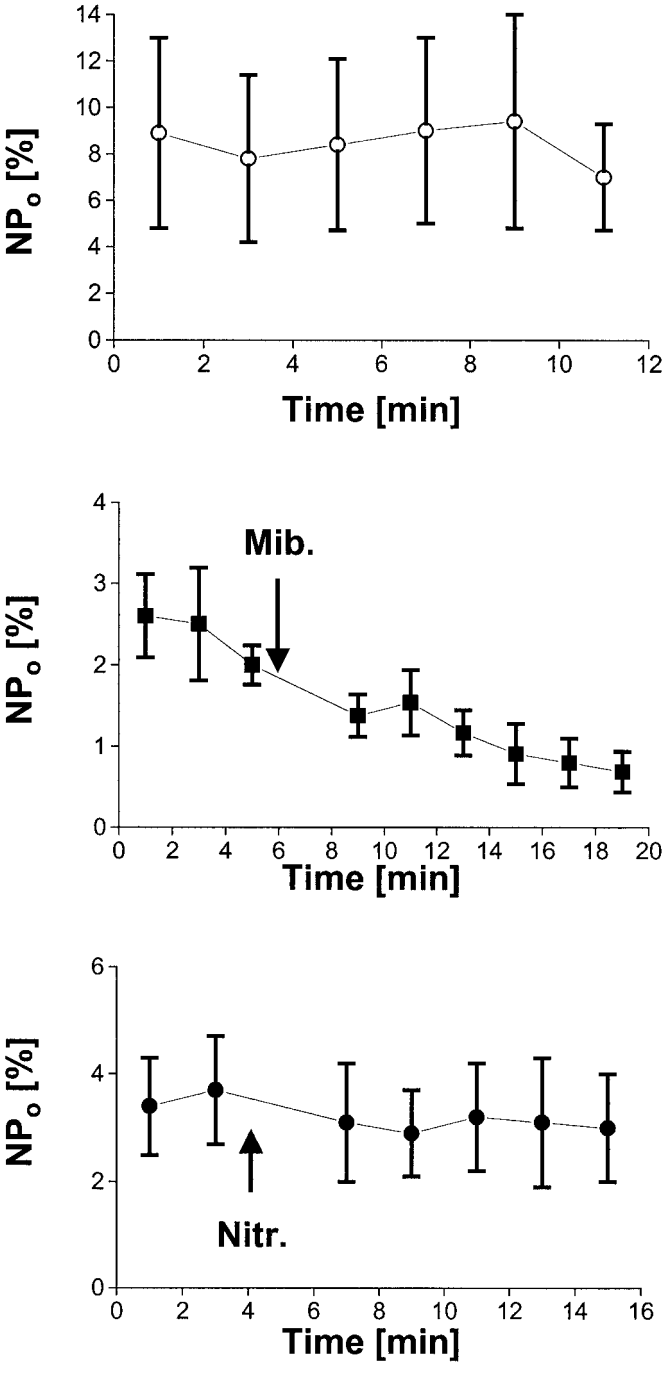

Fig. 14. Open probability NP_o (averaged over 2-min recording periods) of recombinant $Ca_v3.2$ channels versus time. Channels were held at −50 mV and depolarized to −20 mV. They were exposed either to no drug (top, $n = 6$), or to mibefradil after 6 min (middle, 9.3 ± 0.5 μM, $n = 8$), or to nitrendipine after 4 min (bottom, 10.3 ± 0.2 μM, $n = 5$).

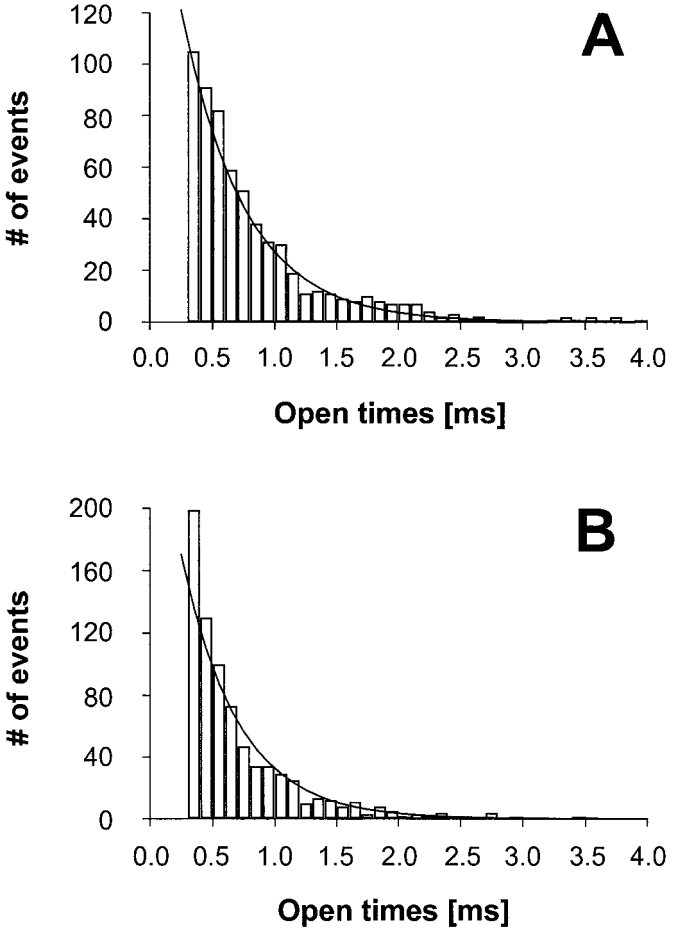

Fig. 15. Open-time histograms from a representative experiment obtained from a $Ca_v3.2$ expressing HEK 293 cell before (A) and after (B) application of 10 μM mibefradil (−50 mV holding potential). τ_{open} obtained from this experiment by maximum likelihood fits decreased from 0.58 ms before to 0.45 ms after drug.

used (150 ms) gave rise to only a few tail openings, which were not further analyzed. The clear-cut two components of the closed-time distribution, with an ultrashort first component, have also been described previously as characteristic for native T-type channels (Droogmans and Nilius, 1989; Chen and Hess, 1990). Based on cloning work (Williams et al., 1999), we suggest that type I channels described here represents the human α1H (or $Ca_v3.2$) isoform in its native environment. Notably, the effect of mibefradil on this channel comprises two components: a major reduction of fraction of active sweeps due to a long-lived interaction and a minor component reflected by a shortening of open times.

This study is the first to examine the single-channel mechanism of mibefradil to block a recombinant human low-voltage–activated calcium channel, $Ca_v3.2$. Unlike the situation with native channels in hMTC cells, the high level of overexpression of channels in HEK 293 cells made it inevitable to perform multichannel recordings. Yet, partial depolarization of the holding potential enabled us to perform a focused analysis of single-channel gating before and after drug application.

Interestingly, mibefradil-induced inhibition again seemed to consist of two components. Blockade that leads to a reduced fraction of active sweeps is indicative for a long-lived drug-channel interaction outlasting the duration of the test pulse (here, 150 ms). This type of effect is known for classical calcium-channel blockade in $Ca_v1.X$, as with gallopamil (Pelzer et al., 1984) or nitrendipine (Hess et al., 1984), and can be analyzed kinetically (Kawashima and Ochi, 1988). In our case, only single-channel patches from hMTC cells allowed such an analysis, revealing a dissociation rate on the order of 0.05/s in the presence of mibefradil (see above). In addition, and in clear kinetic distinction, open times were shortened, which points to another type of interaction on the order of milliseconds and implies open-channel blockade. Of note, Gomora et al. (2000) measured a mibefradil effect of similar size on whole-cell deactivation kinetics, although these authors did not highlight this result. Open-channel block is known for other calcium-channel blockers, at least at high concentrations (Pelzer et al., 1984; Kawashima and Ochi, 1988). Very rapid block in the range of microseconds—which would manifest as a reduced apparent single-channel current amplitude at our recording bandwidth (Hille, 1992)—was absent both in native and recombinant channels (Fig. 16). Such type of block is more common for small pore-blocking particles but has been observed with larger organic molecules (Gingrich et al., 1993).

Largely different time scales of channel block—as seen here—are commonly assigned to different types of channel blockers, each with particular dwell times of binding (Hille, 1992). Because we observed different kinetics within one drug, we may speculate about factors affecting the mechanism of block. The chemical structure of mibefradil contains a benzimidazolyl group and a tertiary amino group. Thus, resulting charge heterogeneity may cause differences in channel interaction (Kass and Arena, 1989; Abernethy, 1997).

We were quite concerned about the high concentrations of mibefradil necessary for an approximately half-maximum block. Given the (sub)micromolar inhibition constant reported for $Ca_v3.2$ under whole-cell conditions (Cribbs et al., 1998; Martin et al., 2000) we provide several lines of evidence that the $\approx$ 10-fold lower affinity of block is still indicative of a specific drug-channel interaction: a dihydropyridine agonist [(*S*)-Bay K 8644] and an antagonist (nitrendipine 10 μM) have no effect in our systems, and mibefradil at a 3-fold lower concentration exerted only minor effects, indicating that we are working in the appropriate range of concentrations. These findings indicate that the low affinity of mibefradil is caused by the particular experimental conditions necessary for single-channel recording. We cannot decide at present whether accessibility limitations imposed by the cell-attached configuration, the high concentration of divalent cations, or both are responsible. The latter mechanism is supported by whole-cell studies (Martin et al., 2000). The former idea is less likely, given the ease of cellular accumulation of mibefradil (Wu et al., 2000), but can be rigorously tested using the inside-out or outside-out excised patch conformation.

HEK 293 cells used in this work overexpress pore-forming $Ca_v3.2$ channel subunits (Cribbs et al., 1998). The existence of endogenous auxiliary subunits cannot be firmly excluded, because native HEK 293 can express endogenous small low-voltage–activated currents under some conditions (Berjukow et al., 1996). However, we consider it unlikely that those subunits are quantitatively sufficient to modulate transfected $Ca_v3.2$. Therefore, we conclude that the natural set of accessory subunits possibly coexpressed (in stoichiometric

TABLE 2

Synopsis of drug effects on recombinant single $Ca_v3.2$ channels

Effects of mibefradil (3.3 ± 0.1 and 9.3 ± 0.5 μM) and nitrendipine (10.3 ± 0.2 μM) on recombinant $Ca_v3.2$ channels. I_{peak}, peak current of the ensemble average current; f_{active}, fraction of active sweeps; and NP_o, total open time/total pulse duration.

	I_{peak}	f_{active}	Mean open time	NP_o	*n*
	fA	%	*ms*	%	
$Ca_v3.2$ (HEK 293)					
control	−58 ± 24	64 ± 15	0.78 ± 0.10	8.7 ± 4.5	6
Second control	−62 ± 25	65 ± 16	0.76 ± 0.08	7.1 ± 2.7	6
$Ca_v3.2$ (HEK 293)					
control	−35 ± 8	61 ± 14	0.84 ± 0.14	4.2 ± 1.0	5
Nitrendipine (10 μM)	−24 ± 4	51 ± 12	0.91 ± 0.26	3.0 ± 0.8	5
$Ca_v3.2$ (HEK 293)					
control	−93 ± 24	88 ± 7	0.72 ± 0.09	11 ± 3.2	6
Mibefradil (3.3 μM)	−69 ± 24*	70 ± 15	0.62 ± 0.09	7 ± 2.9*	6
$Ca_v3.2$ (HEK 293)					
control	−46 ± 5	67 ± 5	0.73 ± 0.09	2.5 ± 0.2	8
Mibefradil (10 μM)	−24 ± 4*	40 ± 5*	0.63 ± 0.08	1.1 ± 0.2*	8

*, a significant effect ($p < 0.05$) between the first and second period.

amounts) with native T-type calcium channels in hMTC cells plays no detectable role with regard to single-channel activity under baseline conditions or to mibefradil block. However, a thorough biophysical analysis of recombinant channels under baseline conditions was hampered by technical limitations of the expression system: holding potentials negative to −50 mV inevitably led to multiple overlapping channel openings (Fig. 12), and test potentials positive to −20 mV could not be analyzed because of inadequate signal-to-noise ratios and insufficient seal stability.

This article presents the first description of mibefradil blockade of native and recombinant $Ca_v3.X$ channels at the single-channel level. We found that mibefradil caused a profound blockade of T-type– and $Ca_v3.2$-mediated calcium channel currents, which consisted of two kinetically distinct components. Our results show that recombinant ($Ca_v3.2$) and native T-type calcium channels share a common pharmacological phenotype as probed by mibefradil. Hence, we conclude that hMTC cells express both T-type and L-type calcium channels, hMTC cells and HEK 293 cells overexpressing the $Ca_v3.2$ subunit are useful tools for single-channel studies on low-voltage–activated calcium channels, offering distinct advantages and limitations, and mibefradil block in both systems reveals two kinetically distinct components at the single-channel level, suggesting two distinct mechanisms of block.

Acknowledgments

We gratefully acknowledge the skillful technical help of Mrs. Sylvia Goitzsch and Mrs. Elke Hippauf. Furthermore we thank Dr. Andreas Jäger for creating the computer program *Patch 0.2*, and Dr. Hartmut Stützer for statistical advice. We appreciate the support from Dr. A. Grauer (University of Heidelberg, Heidelberg, Germany), who generously provided the hMTC cells.

References

Abernethy DR (1997) Pharmacologic and pharmacokinetic profile of mibefradil, a T- and L-type calcium channel antagonist. *Am J Cardiol* **80:**4C–11C.
Bean BP (1985) Two kinds of calcium channels in canine atrial cells. *J Gen Physiol* **86:**1–30.
Berjukow S, Doring F, Froschmayr M, Grabner M, Glossmann H, and Hering S (1996) Endogenous calcium channels in human embryonic kidney (HEK293) cells. *Br J Pharmacol* **18:**748–754.
Bezprozvanny I and Tsien RW (1995) Voltage-dependent blockade of diverse types of voltage-gated Ca^{2+} channels expressed in *Xenopus* oocytes by the Ca^{2+} channel antagonist mibefradil (Ro 40-5967). *Mol Pharmacol* **48:**540–549.
Biagi BA, Mlinar B, and Enyeart JJ (1992) Membrane currents in a calcitonin-secreting human C cell line. *Am J Physiol* **263:**C986–C994.
Cachelin AB, de Peyer JE, Kokubun S, and Reuter H (1983) Ca^{2+} channel modulation by 8-bromocyclic AMP in cultured heart cells. *Nature (Lond)* **304:**462–464.
Carbone E and Lux HD (1984) A low voltage-activated, fully inactivating Ca channel in vertebrate sensory neurons. *Nature (Lond)* **310:**501–502.
Chen C and Hess P (1990) Mechanism of gating of T-type calcium channels. *J Gen Physiol* **96:**603–630.
Cribbs LL, Lee JH, Yang J, Satin J, Zhang Y, Daud A, Barclay J, Williamson MP, Fox M, Rees M, et al. (1998) Cloning and characterization of α_{1H} from human heart, a member of the T-type Ca^{2+} channel gene family. *Circ Res* **83:**103–109.
Dolphin AC, Wyatt CN, Richards J, Beattie RE, Craig P, Lee JH, Cribbs LL, Volsen SG, and Perez-Reyes E (1999) The effect of $\alpha_2\delta$ and other accessory subunits on expression and properties of the calcium channel α1G. *J Physiol (Lond)* **519:**35–45.
Droogmans G and Nilius B (1989) Kinetic properties of the cardiac T-type calcium channel in the guinea-pig. *J Physiol (Lond)* **419:**627–650.

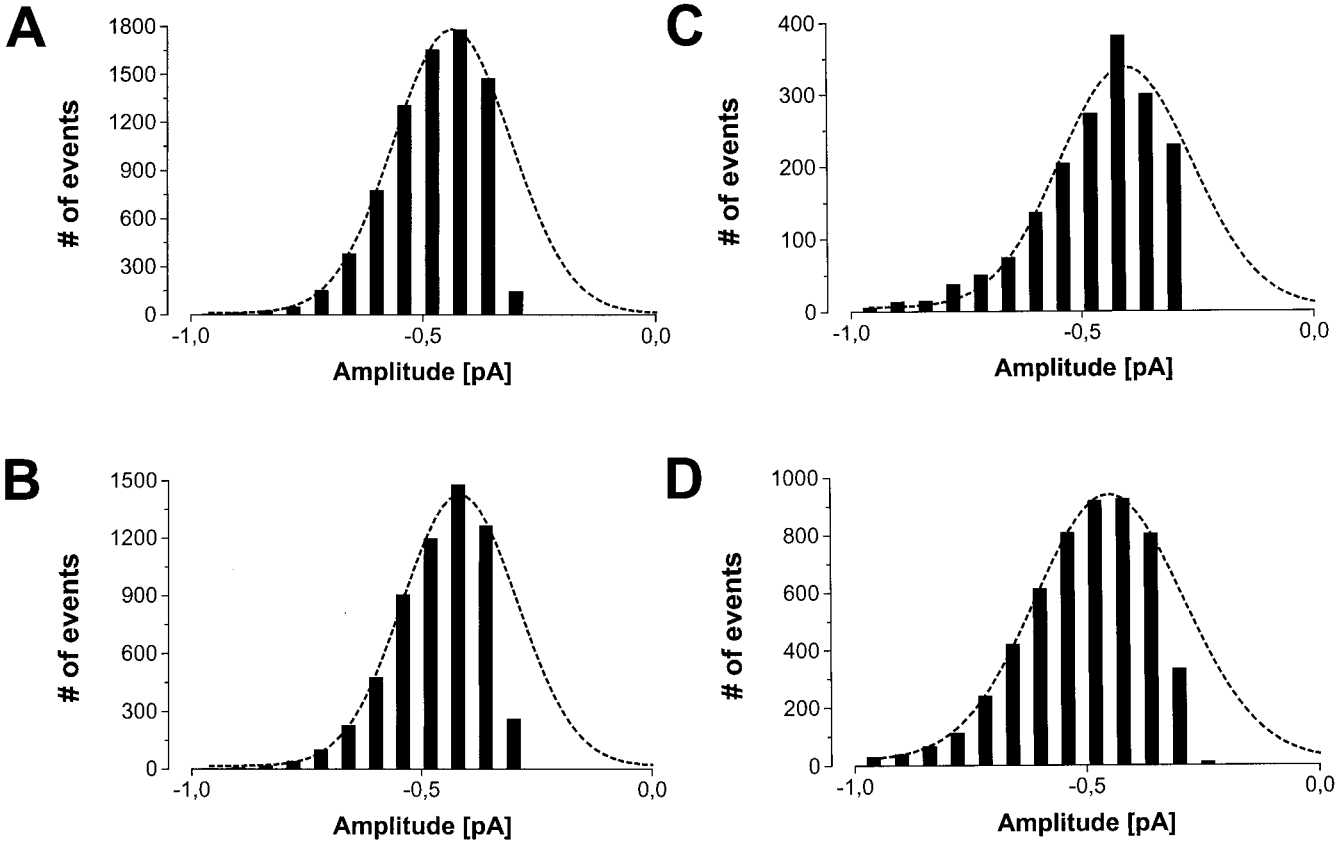

Fig. 16. All-point histograms from two representative experiments obtained from an hMTC cell (A and B) and a Cav3.2 expressing HEK 293 cell (C and D) before (A and C) and after (B and D) application of 10 μM mibefradil. Histograms were constructed from raw data after removing data below the idealization threshold (semi-idealization, see *Materials and Methods*). This inevitably leads to truncation of events below or near the half-height criterion. Mean values obtained by Gaussian fits amounted to −0.43 pA and −0.41 pA (A and B, hMTC) and to −0.41 pA and −0.45 pA (C and D, HEK 293) before and after mibefradil, respectively.

Ertel EA, Campbell KP, Harpold MM, Hofmann F, Mori Y, Perez-Reyes E, Schwartz A, Snutch TP, Tanabe T, Birnbaumer L, et al. (2000) Nomenclature of voltage-gated calcium channels. *Neuron* **25:**533–535.
Gingrich KJ, Beardsley D, and Yue DT (1993) Ultra-deep blockade of Na^+ channels by a quaternary ammonium ion: catalysis by a transition-intermediate state? *J Physiol (Lond)* **471:**319–341.
Gomora JC, Xu L, Enyeart JA, and Enyeart JJ (2000) Effect of mibefradil on voltage-dependent gating and kinetics of T-type Ca^{2+} channels in cortisol-secreting cells. *J Pharmacol Exp Ther* **292:**96–103
Handrock R, Schröder F, Hirt S, Haverich A, Mittmann C, and Herzig S (1998) Single-channel properties of L-type calcium channels from failing human ventricle. *Cardiovasc Res* **37:**445–455.
Herzig S, Patil P, Neumann J, Staschen CM, and Yue DT (1993) Mechanisms of β-adrenergic stimulation of cardiac Ca channels revealed by discrete-time Markov analysis of slow gating. *Biophys J* **65:**1599–1612.
Hess P, Lansman JB, and Tsien RW (1984) Different modes of Ca channel gating behaviour favoured by dihydropyridine Ca agonists and antagonists. *Nature (Lond)* **311:**538–544.
Hille B (1992) *Ionic Channels in Excitable Membranes*, 2nd ed, pp. 391–393, Sinauer, Sunderland, MA.
Hobom M, Dai S, Marais E, Lacinova L, Hofmann F, and Klugbauer N (2000) Neuronal distribution and functional characterization of the calcium channel α2-δ-2 subunit. *Eur J Neurosci* **12:**1217–1226.
Huguenard JR (1996) Low-threshold calcium currents in central nervous system neurons. *Annu Rev Physiol* **58:**329–348.
Kawashima Y and Ochi R (1988) Voltage-dependent decrease in the availability of single calcium channels by nitrendipine in guinea-pig ventricular cells. *J Physiol* **402:**219–235.
Kass RS and Arena JP (1989) Influence of pH_o on calcium channel block by amlodipine, a charged dihydropyridine compound. Implications for location of the dihydropyridine receptor. *J Gen Physiol* **93:**1109–1127.
Klugbauer N, Dai S, Specht V, Lacinova L, Marais E, Bohn G, and Hofmann F (2000) A family of γ-like calcium channel subunits. *FEBS Lett* **470:**189–197.
Kreuzberg U, Theissen P, Schicha H, Schröder F, Mehlhorn U, De Vivie ER, Boknik P, Neumann J, Grohe C, and Herzig S (2000) Single-channel activity and expression of atrial L-type Ca^{2+} channels in patients with latent hyperthyroidism. *Am J Physiol* **278:**H723–H730.
Lacerda AE and Brown AM (1989) Nonmodal gating of cardiac calcium channels as revealed by dihydropyridines. *J Gen Physiol* **93:**1243–1273.
Lacinova L, Klugbauer N, and Hofmann F (1999) Absence of modulation of the expressed calcium channel α1G subunit by $\alpha_2\delta$ subunits. *J Physiol (Lond)* **516:**639–645.
Lee JH, Daud AN, Cribbs LL, Lacerda AE, Pereverzev A, Klöckner U, Schneider T, and Perez-Reyes E (1999) Cloning and expression of a novel member of the low voltage-activated T-type calcium channel family. *J Neurosci* **19:**1912–1921.
McDonald TF, Pelzer S, Trautwein W, and Pelzer DJ (1994) Regulation and modulation of calcium channels in cardiac, skeletal, and smooth muscle cells. *Physiol Rev* **74:**365–507.
Martin RL, Lee JH, Cribbs LL, Perez-Reyes E, and Hanck DA (2000) Mibefradil block of cloned T-type calcium channels. *J Pharmacol Exp Ther* **295:**302–308.
Mehrke G, Zong XG, Flockerzi V, and Hofmann F (1994) The Ca^{++}-channel blocker Ro 40-5967 blocks differently T-type and L-type Ca^{++} channels. *J Pharmacol Exp Ther* **271:**1483–1488.
Mishra SK and Hermsmeyer K (1994) Selective inhibition of T-type Ca^{2+} channels by Ro 40–5967. *Circ Res* **75:**144–148.
Nilius B, Hess P, Lansman JB, and Tsien RW (1985) A novel type of cardiac calcium channel in ventricular cells. *Nature (Lond)* **316:**443–446.
Pelzer D, Cavalie A, and Trautwein W (1984) Guinea-pig ventricular myocytes treated with D600: mechanism of calcium-channel blockade at the level of single channels, in *Recent Aspects in Calcium Channel Antagonism* (Lichtlen PR ed), pp. 3–26, Schattauer, Stuttgart, Germany.
Perez-Reyes E, Cribbs LL, Daud A, Lacerda AE, Barclay J, Williamson MP, Fox M, Rees M, and Lee JH (1998) Molecular characterization of a low-voltage-activated T-type calcium channel. *Nature (Lond)* **391:**896–900.
Raue F, Serve H, Grauer A, Rix E, Scherübl H, Schneider HG, and Ziegler R (1989) Role of voltage-dependent calcium channels in secretion of calcitonin from human medullary thyroid carcinoma cells. *Klin Wochenschr* **67:**635–639.
Sigworth FJ and Sine SM (1987) Data transformation for improved display and fitting of single-channel dwell time histograms. *Biophys J* **52:**1047–1054.
Vassort G and Alvarez J (1994) Cardiac T-type calcium current: pharmacology and roles in cardiac tissues. *J Cardiovasc Electrophysiol* **5:**376–393.
Welling A, Lacinova L, Donatin K, Ludwig A, Bosse E, Flockerzi V, and Hofmann F (1995) Expression of the L-type calcium channel with two different β subunits and its modulation by Ro 40-5967. *Pflueg Arch Eur J Physiol* **429:**400–411.
Williams ME, Washburn MS, Hans M, Urrutia A, Brust PF, Prodanovich P, Harpold MM, and Stauderman KA (1999) Structure and functional characterization of a novel human low-voltage activated calcium channel. *J Neurochem* **72:**791–799.
Wu S, Zhang M, Vest PA, Bhattacharjee A, Liu L, and Li M (2000) A mibefradil metabolite is a potent intracellular blocker of L-type Ca^{2+} currents in pancreatic β-cells. *J Pharmacol Exp Ther* **292:**939–943.

Address correspondence to: Stefan Herzig, M.D., Department of Pharmacology, University of Cologne, Gleueler Straβe 24, 50931 Cologne, Germany. E-mail: stefan.herzig@uni-koeln.de